Parametric Stereotomy Interpolation and Evolutionary Optimization of Semicircular Skew Masonry Arches via Upper Bound Limit Analysis

Mohammad Pourfouladi[1(✉)], Natalia Pingaro[1,2], and Gabriele Milani[1]

[1] Department of Architecture, Built Environment and Construction Engineering, Politecnico di Milano, Milan 20133, Italy
mohammad.pourfouladi@polimi.it

[2] European Centre for Training and Research in Earthquake Engineering , EUCENTRE Foundation, 27100 Pavia, Italy

Abstract. The safety assessment of historic skew masonry arches remains a complex engineering task due to their intricate three-dimensional behavior. The load-bearing capacity of these masonry structures depends directly on their internal stereotomy. Traditionally, construction paradigms like false and logarithmic methods are treated as separate categories. This research introduces a scalar factor α to bridge these distinct construction archetypes. The parametric engine recovers false skew at $\alpha = 0$ and logarithmic layouts at $\alpha = 1$. Hyper-logarithmic configurations are generated when the interpolation factor exceeds the unitary value. The methodology proposed utilizes a custom script and the PoliBrick plugin for geometry generation. Bounding the angular coordinate ensures numerical stability and prevents singularities at the supports. Upper-Bound Limit Analysis evaluates the ultimate load carrying capacity by discretizing the arch into infinitely resistant blocks and rigid-plastic interfaces (mortar joints). This physics-driven solver integrates into a Genetic Algorithm to identify rapidly optimal structural forms that maximize/minimize the load carrying capacity. The limit analysis solver adopts Second-Order Cone Programming to handle a three-dimensional Mohr-Coulomb failure criterion with tension cutoff and compression cap. Specific flow variables (plastic multipliers) characterize plastic dissipation at strength-domain corners. The study processed 2,000 unique individuals across skewness angles of 25° and 45°. Results show a consistent and nearly linear increase in collapse capacity as α rises. Enhanced structural interlocking occurs as joint trajectories shift toward the hyper-logarithmic domain. Maximum collapse loads reached about 1470 kN (25°) and 1190 kN (45°) for the investigated arch models. While 25° arches reach higher load carrying capacities, 45° geometries provide superior mesh regularity. These findings prove in a quantitative fashion the role played by stereotomy in the safety assessment of historic masonry skew arches.

Keywords: Skew Masonry Arches · Parametric Stereotomy · Upper Bound Limit Analysis · Genetic Algorithm · PoliBrick Plugin · Joint Angle Interpolation

© The Author(s), under exclusive license to Springer Nature Switzerland AG 2027
O. Gervasi et al. (Eds.): ICCSA 2026 Workshops, LNCS 16758, pp. 482–498, 2027.
https://doi.org/10.1007/978-3-032-30497-1_29

1 Introduction

The structural assessment of historic masonry infrastructures represents a significant challenge for modern engineering. Single-span skew arches are especially prevalent throughout European railway and road networks. Many of these heritage structures continue to function today (see Fig. 1). Their unusual design allows them to traverse barriers at a variety of non-orthogonal angles. This structural necessity became popular throughout the nineteenth century period of industrial expansion [1]. Unlike traditional squared arches with predictable two-dimensional load paths, skew arches behave three-dimensionally. These systems generate significant lateral thrusts and non-uniform stress distributions. Consequently, they are characterized by highly complex 3D failure mechanisms.



Fig. 1. Left: railway bridge No. 74A, over the Leeds & Liverpool Canal [2]. Right: a skew bridge located in the Allegheny Portage Railroad Historic Site in Pennsylvania [3].

The stereotomy of masonry constructions may affect their ability to carry loads. The geometric configuration of blocks is defined by stereotomy. This arrangement controls the formation of potential failure surfaces inside the arch barrel. It also may dictate the frictional resistance required to prevent blocks from sliding against each other [4].

According to recent studies, construction techniques have a major impact on flexural hinge locations and ultimate capacity [5, 6]. Accurate modeling of these bond patterns is thus vital for any reliable structural assessment.

Historically, three primary structural paradigms have been established for the construction of skew masonry arches [5]. The false skew method utilizes bed joints that are positioned parallel to the supporting abutments. This technique simplifies the stone-cutting process but introduces significant vulnerabilities at higher skew angles. In these geometries, the risk of sliding between voussoirs increases as the skew angle becomes steeper. To preserve the orthogonality of the external surface of the arch, spiral bed joints are employed in the helicoidal method. Alternatively, the logarithmic method provides a mathematical formula to maximize structural stability. To reduce the risk of sliding failure, these joints remain perpendicular to the arch face at all elevations. Figure 2 shows both the false and logarithmic construction techniques chosen for the study in this work. The illustration depicts unrolled geometric developments and their topographical patterns.

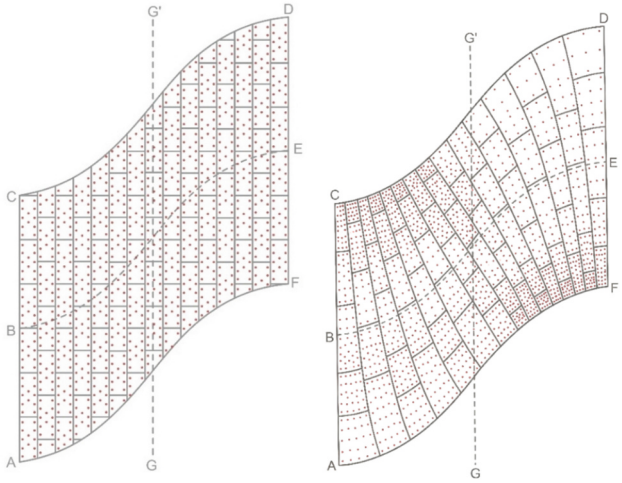


Fig. 2. The unrolled surface pattern of the false and logarithmic skew arches

Contemporary research frequently encounters these three paradigms as distinct and mutually independent groups. This discrete classification limits investigation of the larger structural design space. Furthermore, the literature does not provide a foundation for a continuous mathematical transition between these archetypes. Hybrid setups performance has received little attention in recent research [1, 5]. Previous research has often prioritized canonical approaches above the study of intermediate solutions. A unifying mathematical formulation is crucial for reconciling these methods. Such a model would allow for quantitative optimization of bed-joint trajectories under certain loading conditions.

The current study tackles these constraints by implementing a parametric stereotomy algorithm. This section defines a scalar interpolation factor, α, described in detail in what follows, is defined to bridge traditional construction paradigms. Setting α to zero allows the engine to recover the straight joints of false skew geometry. When α equates one, the framework generates a standard logarithmic layout. Intermediate values between 0 and 1 result in hybrid configurations that combine both strategies. Values greater than one enable "hyper-logarithmic" layouts with increased curvature. (see Fig. 3). This concept is implemented via PoliBrick plugin and custom mathematical code [7].

Structural behavior at collapse is evaluated using a heterogeneous Upper-Bound Limit Analysis (UBLA) code implemented in MATLAB. The procedure discretizes the arch geometry into infinitely resistant hexahedral/wedge elements connected by quadrilateral interfaces. The latter are rigid-plastic and represent either internal block interfaces (infinitely resistant) or mortar joints, where all dissipation takes place according to a cohesive-frictional failure criterion combined with limited tensile and compressive strength (Fig. 4). This Limit Analysis approach serves as a faster alternative to traditional non-linear Finite Element Analyses [8].

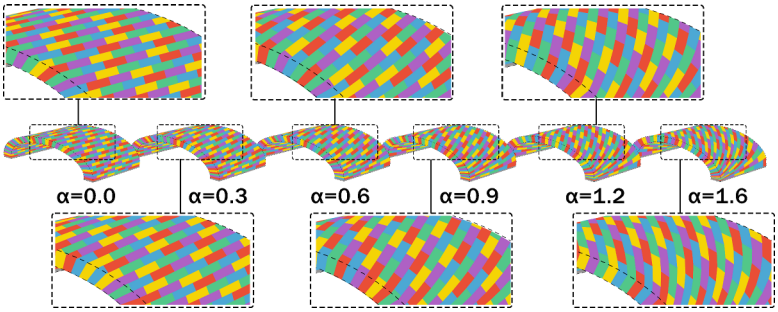


Fig. 3. The role of the interpolation factor in modulating the geometric transition

The limit analysis problem is formulated as a Second-Order Cone Programming (SOCP) task. This method rigorously accounts for frictional contact constraints to identify the collapse load/multiplier. The solver is then integrated into a Genetic Algorithm (GA) for a parametric exploration of the geometry that maximizes/minimizes the ultimate load carrying capacity. This numerical approach identifies the appropriate interpolation coefficient, α. The integrated computational technique discovers high-performance structural combinations across a large design space.

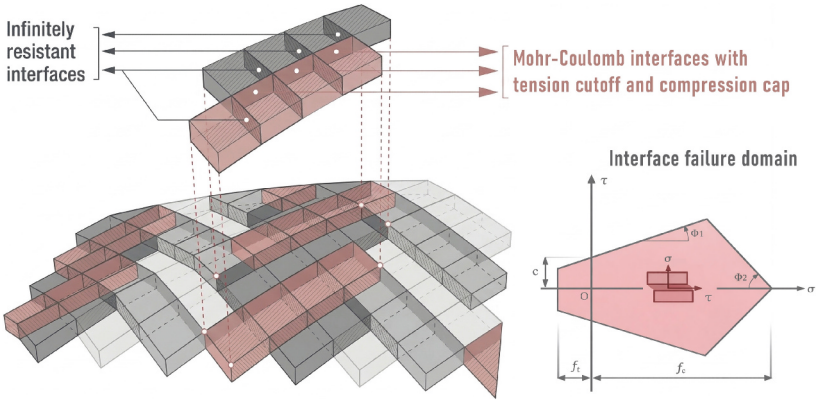


Fig. 4. Geometric discretization at the intersection of block boundaries uses Mohr-Coulomb friction-cohesive interfaces.

Comparative simulations for 25° and 45° skew angles are utilized to determine the role of skewness. Specific geometric measures are used to assess construction complexity and block volume variances. The parametric formulation and optimization strategy are discussed in further detail in subsequent sections. The study finishes by examining the structural impacts of using various building techniques.

2 Methodology

A progressive computational technique combines parametric design and FE-based limit analysis. This method uses an evolutionary search area to identify the optimal structural forms. Using scalar interpolation, the approach merges old archetypes into a single layout. This makes it possible to evaluate the entire design area in a logical and thorough manner. The whole process, from geometry design to performance-based optimization, is shown in Fig. 5 The best configurations are automatically determined by the Genetic Algorithm.

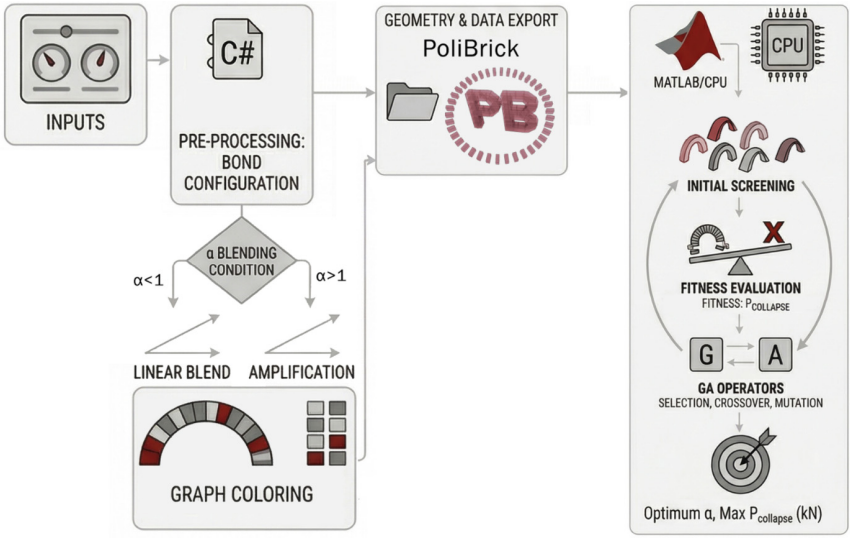


Fig. 5. The skew arch geometry optimization method includes C#-based parametric modeling and GA-driven structural evaluation in MATLAB

2.1 Parametric Geometry Generation

The computational engine for geometry creation is implemented in the Grasshopper environment via a bespoke C# script. It uses the PoliBrick plugin [7] to control discrete assembly and mesh creation processes. Figure 6 shows how the arch shape is determined by a set of predetermined global input parameters. These dimensions include a radius of 2.7 m and a structural thickness of 0.6 m. The voussoir length is fixed at $\ell = 0.75$ m, and the total bridge width is b = 5.0 m. To maintain a width-to-length ratio of around 0.3, 41 courses were used [5].

To maintain a geometrically consistent layout for the 41 courses, the script first performs a numerical integration. This process determines the cumulative arc length S along the mid-surface, where:

$$S = \int_{-\pi/2}^{\pi/2} R_{\text{mid}} \sqrt{\cos^2(u)\cot^2(\omega) + \sin^2(u)}\, du \tag{1}$$

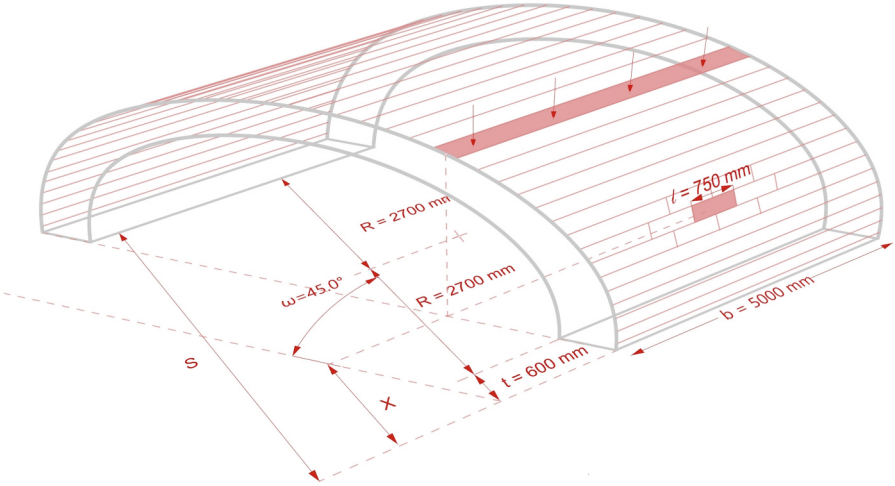


Fig. 6. Geometric specifications of the skew arch for the GA optimization

The variable R_{mid} denotes the radius to the center of the arch thickness, expressed as $(R + t/2)$. The angular coordinate u is measured in radians, ranging from $-\pi/2$ to $+\pi/2$. Furthermore, ω denotes a corresponding skew angle resulting from the bridge orientation. This resulting arc length guarantees equidistant mapping of course borders across any arch skew.

After discretization, the longitudinal trajectory of bed joints with a logarithmic configuration ($\alpha = 1$) is determined. This path is defined by the following analytical equation:

$$y = R_{\text{mid}}\sin(u)\cot(\omega) + R_{\text{mid}}\tan(\omega)\ln(\sec(u) + \tan(u)) + C \tag{2}$$

The variable y indicates the longitudinal position along the barrel depth. To ensure orthogonality on the arch face, the script employs the natural logarithm ln. An integration constant C defines the fixed beginning offset for each course. The range $[-1.56, 1.56]$ radians is the limit of the angular coordinate u.

This kind of bounding avoids singularities at the springing points and guarantees numerical stability. The model employs an interpolation factor $\alpha \in [0,2]$. α is intended as the chromosomal encoding for the Genetic Algorithm. It makes it easier to move continuously between different geometric domains in mathematics. The specific value of $\alpha = 1$ serves as a mathematical baseline that reproduces the traditional logarithmic skew arch. By examining components greater than one, the analysis determines if this historical paradigm is, in fact, the optimal structural solution. Lastly, for every course boundary i, a blended three-dimensional position vector is created. This vector incorporates the transverse position c_2 and the radial distance r. The blended three-dimensional position vector is defined as:

$$\mathrm{P}_\alpha(i, c_2, r) = (1 - \alpha)\mathrm{P}_{\text{false}}(i, c_2, r) + \alpha\mathrm{P}_{\log}(i, c_2, r) \tag{3}$$

where:

i. $P_\alpha = (X_\alpha, Y_\alpha, Z_\alpha)$ is the resulting blended Cartesian position
ii. P_{false} corresponds to the coordinates of a standard false skew arch with straight bed joints
iii. P_{log} corresponds to the optimized logarithmic positions

Note that the spatial mapping inside the conventional interpolation domain ($0 \leq \alpha \leq 1$) is governed by Eq. (3). A straight Cartesian extrapolation using this linear method will provide inconsistent geometric coordinates for shape parameter values greater than 1 (hyper-logarithmic domain), as described below.

The false skew position is computed directly from the uniformly distributed angular coordinate:

$$P_{false} = \begin{pmatrix} r\sin(u_i^{false}) \\ r\sin(u_i^{false})\cot(\omega) + c_2 \\ r\cos(u_i^{false}) \end{pmatrix} \tag{4}$$

The approach intentionally increases the angular deviation in the hyper-logarithmic domain. To establish the spatial position, the script extrapolates data beyond the baseline logarithmic solution:

$$u_{hyper} = u_{false} + \alpha\left(u_{log} - u_{false}\right) \; s.t. \; u_{hyper} \in \left[-\frac{\pi}{2} + \epsilon, \; \frac{\pi}{2} - \epsilon\right] \tag{5}$$

where $\epsilon = 10^{-6}$ prevents numerical singularities. The corresponding spatial position becomes:

$$P_{hyper} = \begin{pmatrix} r\sin(u_{hyper}) \\ r\sin(u_{hyper})\cot(\omega) + c_2 \\ r\cos(u_{hyper}) \end{pmatrix} \tag{6}$$

When compared to the conventional logarithmic model, this formulation increases the curvature of the bed joint. The barrel original extrados and intrados surfaces are effectively preserved.

It is worth mentioning that Eqs. (5–7) allow safe access to the hyper-logarithmic domain ($\alpha > 1$) without generating inconsistencies in the stereotomy of the arches. After generating the three-dimensional geometry, the framework adds taper bricks at the skew faces. This automated process ensures the maintenance of proper masonry bond patterns.

For structural boundary conditions, mesh faces and vertices are identified via an index-mapping process. After that, these elements are ready to be included into the Limit Analysis solver. As shown in Fig. 6, at X/S = 0.3 a vertical linear load is applied. Asymmetric collapse mechanisms common to semicircular masonry arches are triggered by such loads.

2.2 Upper Bound Limit Analysis and SOCP

Heyman's seminal contribution [9], led to significant advancements in the structural analysis of historical arches. Limit analysis for masonry, specifically the safe theorem,

became the primary methodology for evaluating the ultimate capacity of brick-made structures. Subsequent works have enhanced this paradigm through more advanced kinematic simulations that mimic collapse mechanisms via flexural hinge generation [10–14]. Researchers have developed various numerical and analytical methods to study the stability and structural behavior of masonry [15–22]. The kinematic theorem remains popular in the scientific community due to its computing efficiency and straightforward physical explanation. However, the original Heyman assumptions of unlimited compressive strength and negligible friction may be too limiting for complicated three-dimensional designs like skew arches. In such constructions, the angular thrust direction relative to joint planes causes large shear loads, necessitating the explicit consideration of finite friction capacity using Mohr-Coulomb failure criteria rather of the no-sliding idealization. Furthermore, when significant localized compression is combined with shear stress at crucial surfaces, the assumption of infinite compressive strength is called into doubt.

The current technique builds on the kinematic method by discretizing the Masonry structure into infinitely resistant hexahedron and wedge finite elements connected by rigid-plastic interfaces, where all nonlinear behavior is lumped. Unlike traditional formulations that use Linear Programming with piecewise linear yield surface approximations, this study uses a Second-Order Cone Programming (SOCP) solution. This mathematical technique allows for a more rigorous analysis of the three-dimensional Mohr-Coulomb failure criterion, together with a compression cap, eliminating the need for polygonal simplifications of the real yield domain. Milani [10] and Portioli et al. [13] provide comprehensive theoretical underpinnings for indefinitely resistant block limit analysis.

The kinematic variables consist of six degrees of freedom per element, comprising three centroid velocities and three rotation rates. At each interface corner, the SOCP formulation introduces specific plastic flow multipliers to characterize plastic dissipation, see also Fig. 7: one for tension opening (λ_T), one for Mohr-Coulomb sliding, with three components (s_{MC}, δr_{MC}, δq_{MC}), and one for compression cap crushing, again with three components (s_{Cap}, δr_{Cap}, δq_{Cap}). The yield surface combines a modified Mohr-Coulomb criterion with a tension cutoff and a compression cap, expressed through circular Lorentz cones that bound the tangential velocity jumps:

$$\sqrt{(\delta r_{MC})^2 + (\delta q_{MC})^2} \leq s_{MC} \text{ and } \sqrt{(\delta r_{Cap})^2 + (\delta q_{Cap})^2} \leq s_{Cap} \tag{7}$$

Plastic compatibility is preserved through an associated flow rule linking the total velocity jump components at each interface corner to block kinematics. The normal jump is expressed as:

$$\delta n = \mu s_{MC} + \rho s_{Cap} + \lambda_T \tag{8}$$

while the tangential components follow $\delta r = \delta r_{MC} + \delta r_{Cap}$ and $\delta q = \delta q_{MC} + \delta q_{Cap}$. In these expressions, μ denotes the friction coefficient and ρ represents the compression cap shape factor. The internal power dissipation at each corner takes the form:

$$D = c \cdot s_{MC} + f_t \cdot \lambda_T + (\rho \cdot f_c) \cdot s_{Cap} \tag{9}$$

The material parameters adopted in this study are intended to represent a general class of stone masonry with weak joint interfaces. Specifically: friction coefficient $\mu = 0.75$, cohesion $c = 0.015$ MPa, tensile strength $f_t = 0.015$ MPa, compressive strength $= f_c$ 2.5 MPa, compression cap factor $\rho = 0.5$, and density 2700 kg/m^3 which approximates the density of many types of rocks, e.g. andesite. These values ensure that all three failure modes (sliding, hinge opening, and compression crushing) remain potentially active, allowing the optimization to identify the governing mechanism without a priori exclusion. The low cohesion and tensile strength approximate nearly dry-joint conditions while providing numerical regularization.

The collapse load multiplier Λ is determined by minimizing the difference between total internal dissipation and the power of loads independent of the multiplier (i.e., self-weight). The present formulation is developed specifically for the case of applied point loads, where a normalization condition ensures that the power of these loads equals unity, guaranteeing identification of a unique failure mechanism. The complete SOCP problem is formulated as:

$$\min\{\Lambda = \sum_{l=1}^{N_{in}} \sum_{k=1}^{4} D_{lk} - \sum_{i=1}^{N_e} V_i \mathbf{f}_0^{(i)T} \mathbf{U}^{(i)}\} \tag{10}$$

Subject to:

i. Kinematic Consistency: $\mathbf{BU} - \dot{\boldsymbol{\lambda}} = 0$ (Equality constraints for velocity jumps).
ii. Normalization: $\mathbf{P}_{applied}^{T}\mathbf{U} = 1$ (Power constraint ensuring unit virtual work by applied point loads).
iii. Conic Constraints: $\dot{\boldsymbol{\lambda}} \in \mathcal{K}$ (Lorentz cones for MC and Cap, see Fig. 7).
iv. Non-negativity: $\lambda_{MC}, \lambda_{Cap}, \lambda_T \geq 0$.
v. Boundary Conditions: $\mathbf{U} = 0$ at externally constrained elements

where N_{in} denotes the number of interfaces, the index $k = 1, \ldots, 4$ refers to the four corners of each quadrilateral interface,N_e is the number of elements, V_i is the volume of element i, $\mathbf{f}_0^{(i)}$ is the body force density vector (self-weight), $\mathbf{U}^{(i)}$ is the element velocity vector, $\mathbf{B}$ is the kinematic compatibility matrix, $\dot{\boldsymbol{\lambda}}$ collects all interface flow variables, and $\mathcal{K}$ represents the Cartesian product of Lorentz cones enforcing the yield constraints.

This formulation is solved using the MOSEK internal-point optimizer, which provides significantly higher numerical stability and speed compared to standard simplex-based linear solvers. This approach significantly reduces the total number of constraints while maintaining a more accurate representation of the failure surface.

2.3 Evolutionary Optimization via Genetic Algorithm

The approach proposed generates a continuous family of arch geometries indexed by the shape parameter α. Evaluating this entire design space through brute-force methods would be computationally prohibitive, as each structural analysis requires solving a Second-Order Cone Programming (SOCP) problem. Therefore, a Genetic Algorithm (GA) is employed to efficiently search for the specific α value that maximizes (or alternatively minimizes) the total collapse load. Genetic Algorithms effectively optimize

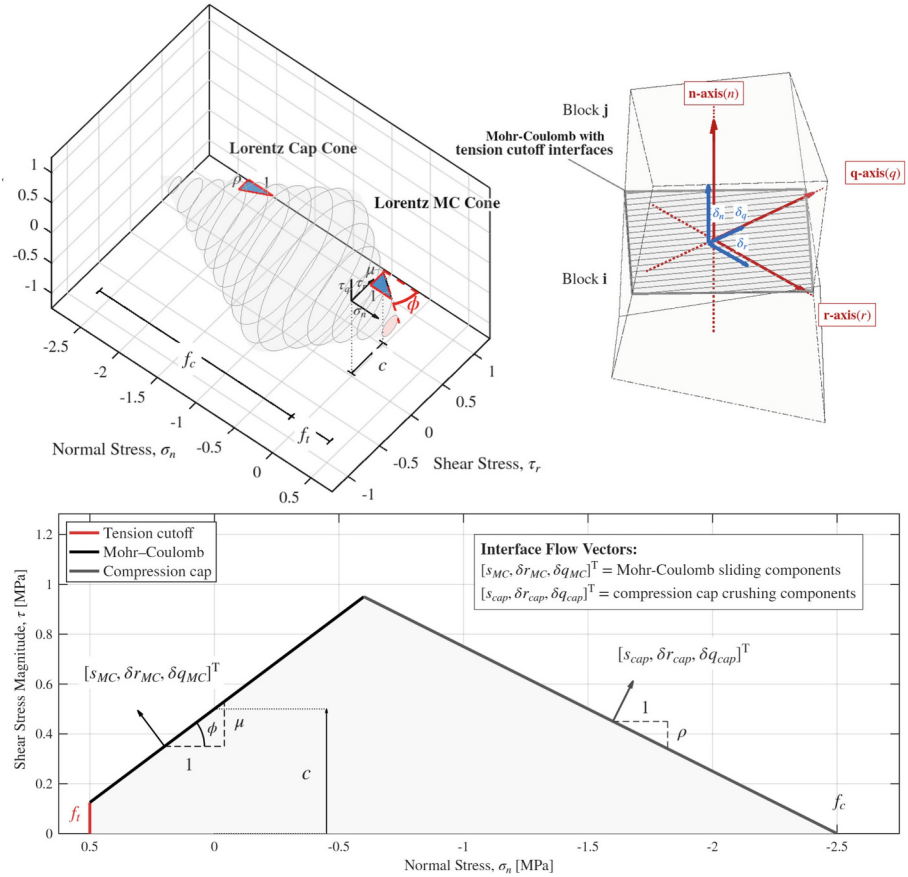


Fig. 7. 3D representation of the yield surface for mortar joints and its 2D cross-section. (Note: The material parameters used to plot the strength domain are the following: $\mu = 0.75$, c = 0.5 MPa, f_t= 0.5 MPa, f_c=2.5 MPa, $\rho = 0.5$. They are purely illustrative and differ from the values used in the actual analyses).

geometries in various engineering fields [24–28]. In masonry research, GAs are frequently paired with limit analysis [26–28]. This combination evaluates structural layouts and potential collapse mechanisms associated with the maximization of the load carrying capacity. The present study uses a GA-based limit analysis to determine quickly the most convenient texture to use for the carrying capacity maximization. Each individual in the GA population encodes a single real-valued chromosome with $\alpha \in [0,2]$. The SOCP solver computes the collapse multiplier Λ, establishing the total collapse load as the fitness metric to rank each candidate geometry:

$$P_{collapse} = \frac{\Lambda \cdot n_{loads}}{1000} \tag{11}$$

In the previous equation,$P_{collapse}$ is the fitness value used to rank individuals.λ is the collapse multiplier calculated by the MOSEK solver.n_{loads} represents the number of

applied point loads. The algorithm also evaluates the variability of the discretization in blocks through the Coefficient of Variation (CV) of the block volumes:

$$CV_{volume} = \frac{\sigma_{vol}}{\mu_{vol}} \tag{12}$$

From a structural and constructability perspective, a lower CV_{volume} indicates a highly uniform mesh where most blocks are of similar size and shape. This uniformity translates practically to a simpler, more repeatable stone-cutting and fabrication process. The parameter CV_{volume} signifies the relative dispersion of the discretization. This metric is defined by the standard deviation σ_{vol} and the mean μ_{vol} of the block volumes. The search begins with 50 candidates that evolve over 30 generations. An elitist strategy preserves the top 5 individuals for the next generation. Selection is performed through a tournament process with a size of 5. The crossover and mutation operators have probability of 0.8 and 0.15, respectively. Finally, a stability check examines convergence across a certain window of generations:

$$\sigma_{best} < \epsilon_{tol} \tag{13}$$

The standard deviation of the maximum collapse load is denoted by σ_{best}, whereas ϵ_{tol} represents convergence.

3 Results

This study uses parametric optimization and geometric sensitivity analysis to determine the gravitational stability of skew arches. The research analyzes two different layouts with 25° and 45° skewness angles. The study analyzed 2,000 distinct people using a Genetic Algorithm and Second-Order Cone Programming.

(SOCP) Framework. This dataset includes 1,000 distinct examples for each level of skewness studied. The comparison study demonstrates that the 25-degree skew arch has a greater maximum collapse load because it maintains geometric integrity throughout a larger design region. When α exceeds 1.6, component dimensions drop below 2 cm, making 45-degree geometry physically impossible. At $\alpha = 0$ and $\alpha = 1.6$, the arch configurations behave similarly. According to the data shown in Fig. 8, the 45-degree arch has somewhat superior performance within the relevant range of 0 to 1.6. Both skewness scenarios show a roughly linear connection between α and the resultant collapse load.

The peak performance measurements for the top-ranked individual are given in the table below (Table 1):

A reference straight arch serves as a baseline. At $\alpha = 0$, this geometry behaves like a typical false skew arch, with a block volume Coefficient of Variation of 0.0743. Figure 9 depicts the thrust line and four-hinge collapse mechanism for this arrangement. At the initial condition, all three arch models have the same collapse load of 362.98 kN. Larger α values do not significantly affect the geometry of a straight arch. In skewed geometries, the logarithmic generation rule causes bed joints to stay perpendicular to the lateral faces; nevertheless, applying this theory to a straight arch yields parallel beds again.

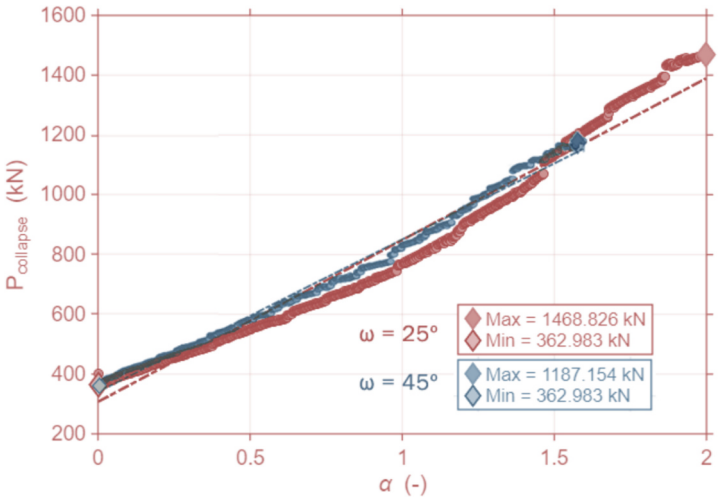


Fig. 8. The analysis of the total collapse load (kN) via the shape parameter α

Table 1. Summary of the optimal configurations for each simulation case

Skewness Angle	Optimal α	Max $P_{collapse}$(kN)	Max Lambda (λ)	N_{loads}	Volume CV
0	–	362.98kN	15,124.29	24	0.0743
25°	1.9980	1,468.83 kN	86,401.51	17	0.5508
45°	1.5760	1,187.15 kN	53,961.56	22	0.3679

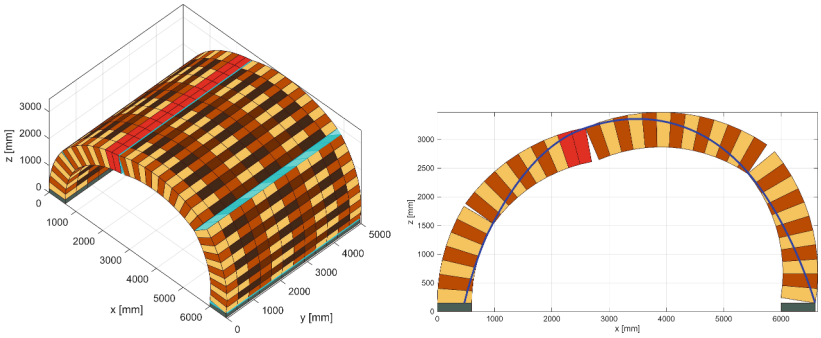


Fig. 9. Thrust line and four-hinge collapse mechanism of a straight arch.

The methodology was validated by comparing the baseline straight arch ($\alpha = 0$) with available literature and manual calculations. With a cohesion and tensile strength of 0.015 MPa, the numerical study showed a collapse load of 362.98 kN. The collapse load dropped to 240.51 kN by applying a 28° friction coefficient and lowering these strength parameters to almost zero to approximate dry-joint conditions ($c \approx 0, f_t \approx 0$).

The analytical calculation of 241.58 kN is supported by this numerical finding. These values are quite similar to the 260 kN ultimate capacity for the same geometry reported in [5]. Additionally, the failure mechanisms of the straight and false skew designs were the same, which is consistent with the behavior reported in [5]. When taken as a whole, these confirmations show that the elevated load capabilities seen in the baseline and hyper-logarithmic models are mathematically consistent.

The collapse mechanisms for several 45-degree skew arch geometries are shown in Fig. 10. The mechanism fails through a standard hinge opening mode at $\alpha = 0$, which denotes the pure false skew arch. The zigzag pattern introduced by the shift toward the logarithmic shape improves structural interlocking. The collapse load increases by almost four times as a result of this geometric shift, from 362.98 kN to 1187.15 kN. The 45-degree arch is still more effective at $\alpha = 1$, but the 25-degree instance shows a similar trend. In the end, after the shape factor surpasses 1.48, the 25-degree design attains superior performance.

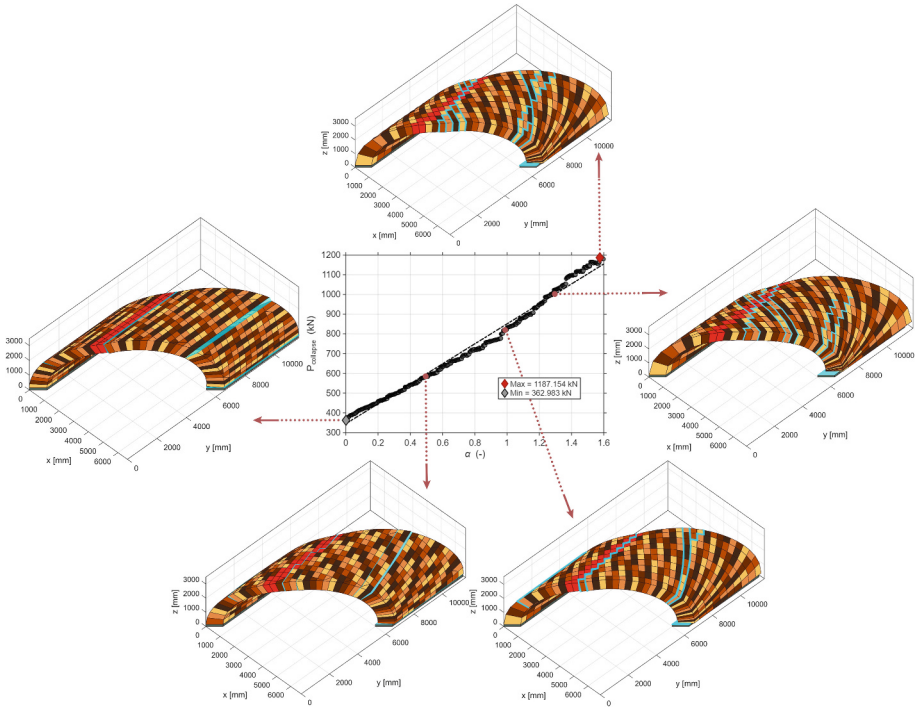


Fig. 10. Variation of collapse mechanism for different geometric shapes

The impact of mesh discretization on structural constructability is revealed by analyzing the Coefficient of Variation (CV) for block volumes. The 45-degree design produces a more uniform mesh ($CV_{volume} = 0.36$) than the 25-degree example ($CV_{volume} = 0.55$), as seen in Fig. 11. Better geometric regularity throughout the masonry components is indicated by lower CV values. This consistency guarantees effective assembly and greatly

streamlines the manufacture process. Furthermore, Fig. 11 illustrates a higher increase in block shape diversity throughout the geometric design space for the 25-degree arch. The data shows that 45-degree arches are more regular and structurally stronger for identical α values when this regularity is correlated with structural capacity.

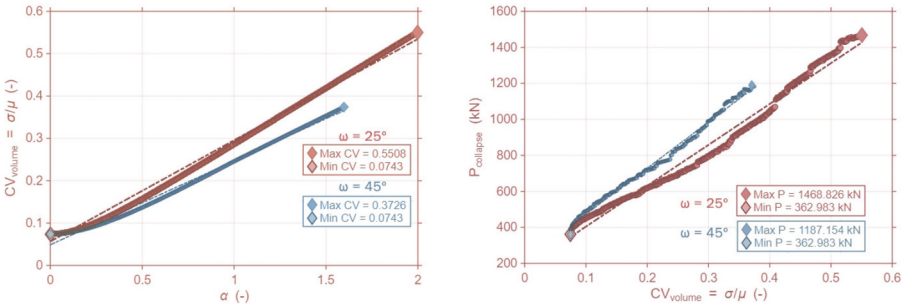


Fig. 11. Distribution of mesh regularity (*CV*) via the geometric shape parameter α and the ultimate collapse load.

The structural effects of changing the vertical interfaces of masonry blocks are assessed in a focused sub-study. This analysis compares vertical joints that stay precisely parallel to the arch face versus those that use an interpolation rule while maintaining a consistent bed joint trajectory. The resulting geometric shift is shown in Fig. 12, which shows parallel joints in red and interpolated vertical joints in gray.

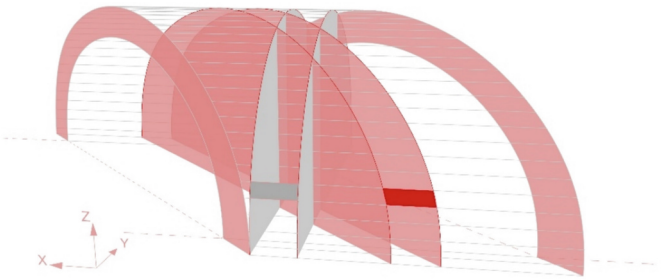


Fig. 12. Visual comparison highlights how vertical interface orientation influences the overall masonry arrangement.

Figure 13 exhibits how altering the vertical joint position results in almost the same collapse mechanisms over a range of α values. The analysis isolates this geometric variable by keeping the bed joint trajectory constant for a given shape parameter. The numerical approach proposed then evaluates the load carrying capacities of arches with vertical joints parallel to the arch face against those utilizing an angular interpolation rule. Specific visual comparisons of the failure mechanisms for $\alpha = 0$ and $\alpha = 0.5$ clearly confirm this consistent structural behavior. Ultimately, altering the vertical cross

joints does not significantly modify the overall failure mode or the hinge locations within the masonry assembly. Despite the consistent failure mechanisms, transitioning to interpolated joints significantly lowers load carrying capacity. For $\alpha = 0$ case, the collapse load drops from 487 kN to 362 kN under the interpolation rule. A similar trend appears in the second case where α is equal to 0.5. Here, the capacity decreases from 817 to 608 kN following the change in joint geometry. These results confirm the intuitive statement that using smaller blocks, failure loads decrease (because more interfaces where plastic dissipation may occur are present).

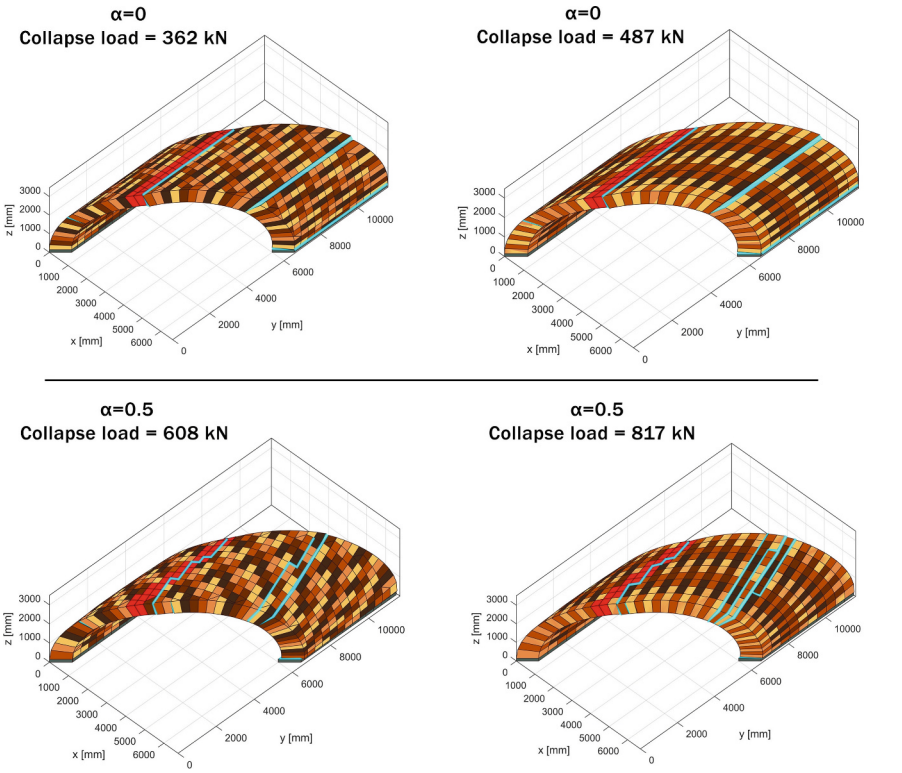


Fig. 13. Failure mechanisms for different vertical joint configurations: interfaces governed by the α interpolation rule (left) alongside interfaces parallel to the arch face (right).

4 Conclusion

Historically, skew masonry arch construction techniques have been divided into discrete groups by engineers. The most well-known instances of these traditional methods are the false and logarithmic layouts. In order to overcome this conceptual division, the study presents a single mathematical formulation. The suggested paradigm creates a seamless geometric transition between “false” and “logarithmic” layouts by using a continuous form parameter. In the end, this process combines several traditionally distinct stone-cutting methods into an all-encompassing structural framework. The study

unites traditional archetypes and investigates superior hyper-logarithmic configurations by introducing the interpolation factor α. Three-dimensional friction, tension, and compression at the inter-block interfaces are rigorously handled by the SOCP-based limit analysis. The findings show that, in comparison to conventional layouts, increasing joint curvature delivers a nearly fourfold improvement in collapse capacity. In the hyper-logarithmic domain, optimal configurations are always discovered when α values are greater than the traditional boundary. The 45° version retains better geometric regularity and manufacture feasibility whereas the 25° version reaches larger peak loads. Additionally, the study demonstrates that structural strength is strongly impacted by the position of vertical cross joints. In particular, the load-carrying capacity is increased when joints parallel to the arch face are used instead of interpolated joints. Interestingly, this performance boost happens despite the failure mechanisms staying the same. This framework provides an effective means of maintaining and improving the structural integrity of aged masonry transit networks. The application of this technique to intricate multi-span skew geometries and experimental validation should be the main goals of future improvements.

References

1. Forgács, T., Sarhosis, V., Bagi, K.: Minimum thickness of semi-circular skewed masonry arches. Eng. Struct. **140**, 317–336 (2017)
2. Skew Arch Bridge, Plane 6, Allegheny Portage RR (Wikimedia Commons). http://commons.wikimedia.org/wiki/File:Skew_Arch_Bridge,_Plane_6,_Allegheny_Portage_RR.jpg. Accessed 25 March 2026
3. Allegheny Portage Railroad - Skew Arch Bridge (Flickr). http://www.flickr.com/photos/141239321/16600585712/in/photostream/. Accessed 25 March 2026
4. Pingaro, N., Milani, G.: Simple interface element equipped with thickness for the non-linear static heterogeneous analysis of masonry walls in-plane loaded: Implementation and validation. Eng. Struct. **351**, 122056 (2026)
5. Forgács, T., Sarhosis, V., Bagi, K.: Influence of construction method on the load bearing capacity of skew masonry arches. Eng. Struct. **168**, 612–627 (2018)
6. Pourfouladi, M., Pingaro, N., Milani, G.: Collapse risk assessment of long-span masonry cloister vaults under paradigmatic crown loading: a heterogeneous limit analysis approach with stereotomy. In: Lecture Notes in Civil Engineering, pp. 123–134. Springer (2025)
7. Pourfouladi, M., Pingaro, N., Valente, M.: PoliBrick plugin as a parametric tool for digital stereotomy modelling. Comput. Struct. **311**, 107722 (2025)
8. Meloni, G., Pourfouladi, M., Pingaro, N.: Parametric modelling and nonlinear FE analysis of Trepponti Bridge subjected to differential settlements. Buildings **16**(1), 47 (2026)
9. Heyman, J.: The stone skeleton. Int. J. Solids Struct. **2**, 249–279 (1966)
10. Milani, G.: 3D upper bound limit analysis of multi-leaf masonry walls. Int. J. Mech. Sci. **50**, 817–836 (2007)
11. Pingaro, N., Milani, G., Tiberti, S.: Automatic CAD kinematic limit analysis approach for the limit analysis of masonry towers. In: AIP Conference Proceedings, vol. 2293, p. 380005. AIP Publishing (2020)
12. Cascini, L., Gagliardo, R., Portioli, F.: LIABlock_3D: a software tool for collapse mechanism analysis of historic masonry structures. Int. J. Architect. Heritage **14**, 75–94 (2018)
13. Portioli, F., Casapulla, C., Gilbert, M., Cascini, L.: Limit analysis of 3D masonry block structures with non-associative frictional joints using cone programming. Comput. Struct. **143**, 108–121 (2014)

14. Hua, Y., Milani, G.: Rigid block limit analysis of masonry arches with associated and non-associated slides. Research for Development, pp. 169–203 (2022)
15. Angelillo, M., Montanino, A., Pandolfi, A.: On the connection between geometry and statically determined membrane stresses in the human cornea. J. Biomech. Eng. **142**(5), 051006 (2020)
16. Perelli, F.L., De Gregorio, D., Montanino, A., Olivieri, C., Maddaloni, G., Iannuzzo, A.: Energy-based modelling of in-plane fragility curves for the 2D ultimate capacity of Italian masonry buildings. Front. Built Environ. **9**, 1127523 (2023)
17. Cusano, C., Montanino, A., Olivieri, C., Paris, V., Cennamo, C.: Graphical and analytical quantitative comparison in the domes assessment: the case of san francesco di paola. Appl. Sci. **11**(8), 3622 (2021)
18. Galassi, S., Ruggieri, N., Tempesta, G.: Ruins and archaeological artifacts: vulnerabilities analysis for their conservation through the original computer program BrickWORK. In: Aguilar, R., Torrealva, D., Moreira, S., Pando, M.A., Ramos, L.F. (eds.) Structural Analysis of Historical Constructions. RILEM Bookseries, vol. 18. Springer, Cham (2019). https://doi.org/10.1007/978-3-319-99441-3_197
19. Galassi, S., Ruggieri, N., Tempesta, G.: A novel numerical tool for seismic vulnerability analysis of ruins in archaeological sites. Int. J. Architect. Heritage **14**(1), 1–22 (2020)
20. Galassi, S., et al.: Digital survey and structural investigation on the triumphal arch of caracalla in the archaeological site of volubilis in Morocco. Int. J. Architect. Heritage **16**(6), 940–955 (2022)
21. Iannuzzo, A., Matarazzo, G., Cusano, C., Ferraro, M., Maddaloni, G.: Insights into the collapse of the asciello masonry bridge in Benevento. In: Gervasi, O., et al. (eds.) Computational Science and Its Applications – ICCSA 2025 Workshops. ICCSA 2025. LNCS, vol. 15886. Springer, Cham (2026). https://doi.org/10.1007/978-3-031-97576-9_26
22. Fabbrocino, F., Olivieri, C., Luciano, R., Vaiano, G., Maddaloni, G., Iannuzzo, A.: Seismic performance of historic masonry buildings: a comparative analysis of equivalent frame and block-based methods. Alex. Eng. J. **109**, 359–375 (2024)
23. Wang, P., Milani, G.: Specialized 3D distinct element limit analysis approach for a fast seismic vulnerability evaluation of massive masonry structures: application on traditional pagodas. Eng. Struct. **282**, 115792 (2023)
24. Buzzetti, M., Milani, G.: Combined genetic algorithm and limit analysis approach for the optimal design of tie rods in historical masonry structures. In: COMPDYN Proceedings, pp. 1002–1012 (2025)
25. Fard, M.S., Ghaderi, E., Pourfouladi, M.: Free-form grid structure multi-objective optimization associated with integrated design and machine learning. Eng. Struct. **329**, 119827 (2025)
26. Nouri, L., Azari, K.T., Pourfouladi, M., Keramat, D., Alaghmandan, M.: Form-finding and optimization of branching columns using L-systems in early stages of design: a parametric approach. J. Build. Eng. **117**, 114817 (2025)
27. Chiozzi, A., Milani, G., Tralli, A.: A genetic algorithm NURBS-based new approach for fast kinematic limit analysis of masonry vaults. Comput. Struct. **182**, 187–204 (2016)
28. Tiberti, S., Grillanda, N., Mallardo, V., Milani, G.: A genetic algorithm adaptive homogeneous approach for evaluating settlement-induced cracks in masonry walls. Eng. Struct. **221**, 111073 (2020)